LYAPUNOV EXPONENTS OF THE KURAMOTO–SIVASHINSKY PDE

RUSSELL A. EDSON[1], J. E. BUNDER[1], TRENT W. MATTNER[1] and
A. J. ROBERTS[1]

Abstract

The Kuramoto–Sivashinsky equation is a prototypical chaotic nonlinear partial differential equation (PDE) in which the size of the spatial domain plays the role of a bifurcation parameter. We investigate the changing dynamics of the Kuramoto–Sivashinsky PDE by calculating the Lyapunov spectra over a large range of domain sizes. Our comprehensive computation and analysis of the Lyapunov exponents and the associated Kaplan–Yorke dimension provides new insights into the chaotic dynamics of the Kuramoto–Sivashinsky PDE, and the transition to its one-dimensional turbulence.

1. Introduction

The Kuramoto–Sivashinsky partial differential equation (PDE) models a wide variety of nonlinear systems with intrinsic instabilities, such as wave propagation in chemical reaction–diffusion systems [21], the velocity of laminar flame front instabilities [29], thin fluid film flow down inclined planes [30], and hydrodynamic turbulence [6, 15, 24]. In the Kuramoto–Sivashinsky PDE the large-scale dynamics is dominated by a destabilizing "diffusion", whereas small-scale dynamics is dominated by stabilizing hyperdiffusion, and a nonlinear advective term stabilizes the system by transferring energy from the large unstable modes to the small stable modes [32, p. 199]. The interplay between these contrasting features leads to significant spatio-temporal complexity [4, 5, 16, 17], from intermittent disorder, through to chaos and turbulence: "turbulence" in the Kuramoto–Sivashinsky PDE is typically described as weak, incipient or localized, rather than fully turbulent; however, this regime provides mathematical insights into the transition from dynamical chaos to true turbulence [17, 24]. Lyapunov exponents characterize this chaos and turbulence [8, 27, 34],

---

[1]School of Mathematical Sciences, University of Adelaide, South Australia, Australia;
e-mail: russell.edson@adelaide.edu.au, judith.bunder@adelaide.edu.au, trent.mattner@adelaide.edu.au, anthony.roberts@adelaide.edu.au.

and are increasingly used to analyse such spatio-temporal complexity in various applications such as turbulent Poiseuille flow [19], turbulence in flames [14] and Rayleigh–Bérnard fluid convection [2, 36].

Here we extend previous research by Manneville [23] and by Tajima and Greenside [33] by discovering new details of how the dynamics of the Kuramoto–Sivashinsky PDE becomes increasingly chaotic as the size of the domain increases, for both periodic and odd-periodic boundary conditions. To measure the degree of chaos, Section 3 computes the Lyapunov exponents using the classic algorithm introduced by Benettin et al. [1] and Shimada and Nagashima [28], but now in new detail over a comprehensive range of domain sizes. By comparison, Tajima and Greenside [33] explored the Kuramoto–Sivashinsky PDE (2.1) with rigid boundary conditions over a range of domain lengths, whereas we explore periodic (2.2) and odd-periodic (2.3) cases, we use an order of magnitude increased resolution in the domain lengths, and we also cover the transition to chaos regime. The Lyapunov exponents describe the rate at which neighbouring trajectories diverge under a chaotic flow, and thus provide a quantitative measure of the degree of chaos in a system. Section 3 analyses the growth of the Lyapunov exponents with increasing domain size, and then uses the Lyapunov spectra to identify the onset of chaos and to characterize new details of the increasingly complex spatio-temporal dynamics of the Kuramoto–Sivashinsky PDE.

A further use of the Lyapunov exponents is in defining the Kaplan–Yorke dimension of the attractor of a dynamical system [18]. The Kaplan–Yorke dimension bounds above the fractal dimension of the chaotic attractor, and approximates the number of effective modes necessary to describe the dynamics on the attractor [12]. For a Kuramoto–Sivashinsky PDE defined on either a periodic or odd-periodic domain, Section 4 confirms more accurately how the Kaplan–Yorke dimension scales roughly linearly with the domain size. This linear scaling corresponds well with the scaling observed by Manneville [23] and Tajima and Greenside [33] for the Kuramoto–Sivashinsky PDE with rigid boundary conditions.

Our detailed analysis of the chaotic dynamics of the Kuramoto–Sivashinsky PDE and its dependence on domain size provides new insights into the onset of chaos. In many chaotic systems, we can identify that discrete point at which a bifurcation parameter permits chaos, but our new visualization of the comprehensive computation of Lyapunov exponents highlights the gradual changes which drive a system into the chaotic regime, and thence into one-dimensional turbulence.

2. The Kuramoto–Sivashinsky equation

On the spatial domain $0 \leq x \leq L$ for some domain size L, the one-dimensional Kuramoto–Sivashinsky PDE for field $u(x, t)$ is

$$\partial_t u + \partial_x^4 u + \partial_x^2 u + u\partial_x u = 0. \tag{2.1}$$

We apply either periodic boundary conditions,

$$u(x + L, t) = u(x, t) \quad \text{for all } 0 \leq x \leq L, \tag{2.2}$$

or odd-periodic boundary conditions,

$$u(x,t) = \partial_x^2 u(x,t) = 0 \quad \text{at } x = 0, L. \tag{2.3}$$

In the Kuramoto–Sivashinsky PDE, the second-order diffusive term $\partial_x^2 u$ is destabilizing, whereas the fourth-order hyperdiffusion term $\partial_x^4 u$ is stabilizing, resulting in large-scale instabilities and small-scale dissipation, with the transfer of energy from large to small scales mediated by the nonlinear term $u\partial_x u$, producing a stabilizing influence on the system [32, p. 199].

The Kuramoto–Sivashinsky PDE (2.1) supports several symmetries, although in the turbulent regime they only hold in a time-averaged sense [5, 35]. Of particular interest for periodic domains (2.2) are the Galilean invariance, $u(x,t) \to u(x - ct, t) + c$ for all speeds c, and the spatial translation invariance, $u(x,t) \to u(x + d, t)$ for all d. These two symmetries do not hold for odd-periodic domains (2.3). The Kuramoto–Sivashinsky PDE (2.1) with odd-periodic domains (2.3) is particularly well studied [9, 10, 22, 25] compared to that with periodic domains, as the removal of periodic symmetries simplifies somewhat the analysis of the dynamics. The relatively simpler dynamics of the odd-periodic case is observed in Section 3 when comparing the periodic and odd-periodic Lyapunov spectra. The most obvious point of difference is that the Galilean and translation invariances support two zero Lyapunov exponents which are absent from the Lyapunov spectra for the odd-periodic case. Commonly for the periodic case, a zero mean condition is imposed to remove the Galilean invariance and consequently one of the zero Lyapunov exponents [5, 6, 35]; we do not impose the zero-mean condition.

As the size L of the spatial domain varies, the Kuramoto–Sivashinsky PDE (2.1) produces distinctly different dynamics [4, 5, 16]. For periodic boundary conditions (2.2), Figure 1 shows the increasing complexity of the Kuramoto–Sivashinsky dynamics as domain size L increases, from a stable travelling wave when $L \lesssim 13$ through to spatio-temporal chaotic turbulence when $L \approx 100$. Figure 2 for the odd-periodic boundary conditions (2.3) also shows an increase in the complexity of the dynamics as L increases, progressing from an oscillating cell when $L \lesssim 17$ through to spatio-temporal turbulence when $L \approx 100$. For both types of boundary conditions, the spatial domain size L plays the role of a bifurcation parameter.

Our aim is to provide new details of the character of the trend to spatio-temporal complexity and "turbulence" with increasingly long domains L. To do this, Section 3 comprehensively computes the 24 most positive (that is, the largest) Lyapunov exponents across a significant range of domain lengths L. It is these most positive Lyapunov exponents which determine the nature of the chaotic dynamics. Then Section 4 evaluates the Kaplan–Yorke dimension over the same range of L to show that the dimension of the chaotic attractor grows linearly with L.

3. Evaluating the Lyapunov exponents

In a dynamical system, the Lyapunov exponents measure the exponential divergence of initially close trajectories, with positive Lyapunov exponents indicating
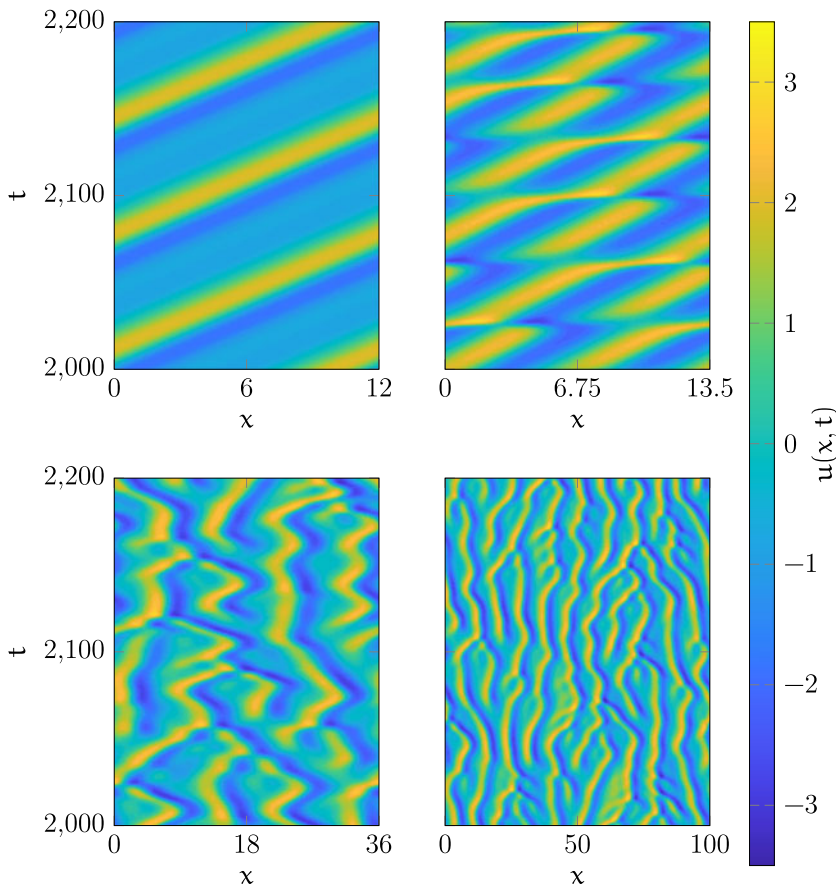
FIGURE 1. Simulations of the Kuramoto–Sivashinsky PDE (2.1) with (2.2) depend upon the size of the periodic spatial domain L: (top left) for $L = 12$, a travelling wave emerges; (top right) for $L = 13.5$, intermittent bursts disrupt the travelling wave structure; (bottom left) for $L = 36$, chaotic cellular structures criss-cross and interact; and (bottom right) for $L = 100$, spatio-temporally complex patterns of "turbulence" occur. Each simulation is shown over the same time range.

divergent trajectories and negative Lyapunov exponents indicating convergence [3, 8]. A chaotic system, due to its sensitivity to initial conditions, must have at least one positive Lyapunov exponent. Furthermore, an increasingly chaotic system has an increasing number of positive Lyapunov exponents. This section evaluates Lyapunov exponents of the Kuramoto–Sivashinsky PDE (2.1) for increasing domain size L, and interprets each increase in the number of positive Lyapunov exponents as a transition to an increasingly chaotic system.

Formally, Lyapunov exponents measure trajectory divergences in the infinite time limit, with different Lyapunov exponents corresponding to divergences in different orthogonal directions. The existence of these time limits is ensured (almost
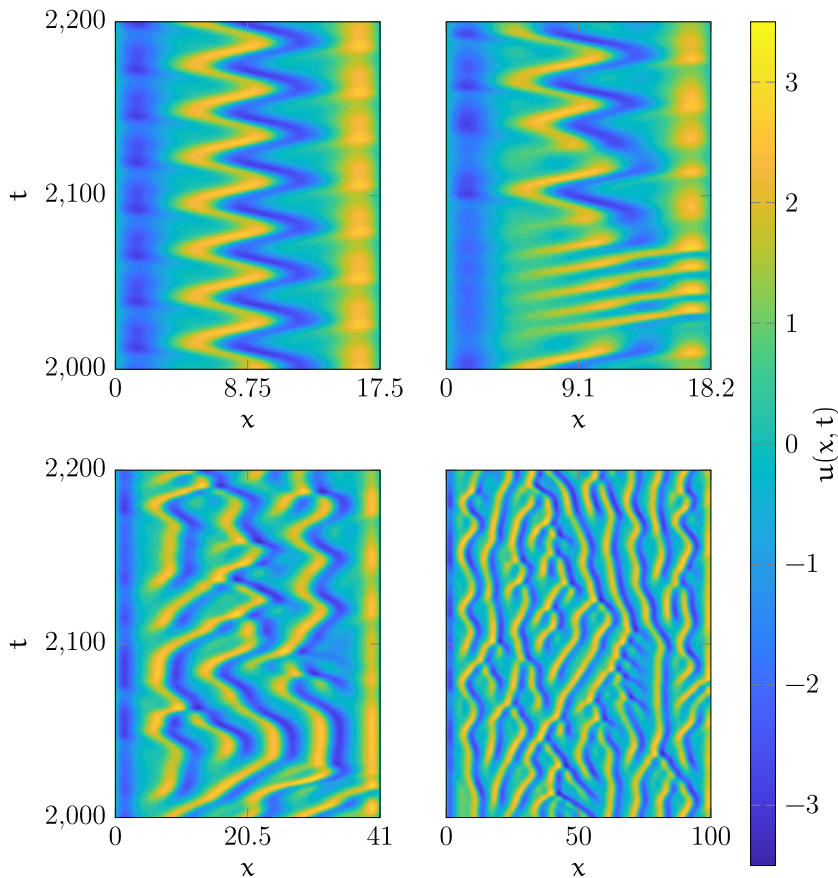
FIGURE 2. Simulations of the Kuramoto–Sivashinsky PDE (2.1) with (2.3) depend upon the size of the odd-periodic spatial domain L: (top left) for $L = 17.5$, an oscillating cell emerges; (top right) for $L = 18.2$, intermittent bursts disrupt the cell structure; (bottom left) for $L = 41$, chaotic cellular structures criss-cross and interact; and (bottom right) for $L = 100$, spatio-temporally complex patterns of "turbulence" occur. Each simulation is shown over the same time range.

everywhere) by Oseledec's multiplicative ergodic theorem [8, 26]. In numerical calculations of Lyapunov exponents, complications due to the infinite time limit are avoided by computing N iterations of the divergence of trajectories over finite time intervals T, with N large but finite [1, 7, 11, 28, 31]. At the end of each iteration, the divergent trajectories are reorthonormalized. This reorthonormalization ensures that the tracked directions remain orthogonal, rather than all converging to that of the largest positive Lyapunov exponent [11]. This rescaling is valid in the ergodic case, because the Lyapunov exponents are (almost everywhere) independent of a trajectory's initial condition. However, the finite-time numerical approximation generally results in some numerical error (for example, [7]).

Algorithm 1 assumes that the vector function of time $\mathbf{u}(t) \in \mathbb{R}^n$ satisfies the dynamical system

$$\dot{\mathbf{u}} = \mathbf{f}(t, \mathbf{u}), \tag{3.1}$$

with initial condition $\mathbf{u}(0)$. Trajectories are first evolved for time τ to ensure initial transients have decayed and thus that the system is close to an attractor. Then Algorithm 1 numerically solves the ordinary differential equation (ODE) (3.1) for a time $N \cdot T$ to compute the m most positive Lyapunov exponents λ_i for $i = 1, \ldots, m \leq n$ using reduced QR decomposition to reorthonormalize after each of N time intervals of length T [1, 7, 11, 28, 31]. As is standard, the resulting Lyapunov exponents are ordered such that $\lambda_1 \geq \lambda_2 \geq \cdots \geq \lambda_m$.

Algorithm 1 The classic algorithm for computing the spectrum of Lyapunov exponents for a dynamical system, introduced by Benettin et al. [1], and Shimada and Nagashima [28].

$d\mathbf{u}/dt = \mathbf{f}(t, \mathbf{u})$: the dynamical system ODE
$\mathbf{u}(0)$: the initial value of $\mathbf{u}$
m: the number of the most positive exponents to compute
τ: time to simulate system before computing exponents
T: time between reorthonormalization steps
N: the total number of reorthonormalization steps
ϵ: perturbation magnitude (typically take $\epsilon = 10^{-6}$).

OUTPUT:

λ_i: the m most positive Lyapunov exponents, $i = 1, \ldots, m$.

1: compute $\mathbf{u}^{(0)} := \mathbf{u}(\tau)$ via solving ODE on $[0, \tau]$
2: set $t_j := \tau + jT$, for $j = 0, 1, 2, \ldots, N$
3: choose initial orthogonal directions $Q^{(0)} := \begin{bmatrix} \mathbf{q}_1^{(0)} & \cdots & \mathbf{q}_m^{(0)} \end{bmatrix}$
4: **for** $j = 1 : N$ **do**
5:     compute $\mathbf{u}^{(j)} := \mathbf{u}(t_j)$ via solving ODE with $\mathbf{u}(t_{j-1}) = \mathbf{u}^{(j-1)}$
6:     **for** $i = 1 : m$ **do**
7:         compute $\mathbf{w}_i^{(j)} := \mathbf{u}(t_j)$ via ODE with $\mathbf{u}(t_{j-1}) = \mathbf{u}^{(j-1)} + \epsilon\, \mathbf{q}_i^{(j-1)}$
8:         approximate $\Psi(t_j, t_{j-1})\mathbf{q}_i^{(j-1)} := (\mathbf{w}_i^{(j)} - \mathbf{u}^{(j)})/\epsilon$
9:     **end for**
10:     construct $\Psi(t_j, t_{j-1})Q^{(j-1)} := \begin{bmatrix} \Psi(t_j, t_{j-1})\mathbf{q}_1^{(j-1)} & \cdots & \Psi(t_j, t_{j-1})\mathbf{q}_m^{(j-1)} \end{bmatrix}$
11:     compute $Q^{(j)}R^{(j)} :=$ QR$(\Psi(t_j, t_{j-1})Q^{(j-1)})$
12: **end for**
13: **for** $i = 1 : m$ **do**
14:     compute $\lambda_i := \sum_{j=1}^{N} \log R_{i,i}^{(j)}/(NT)$
15: **end for**
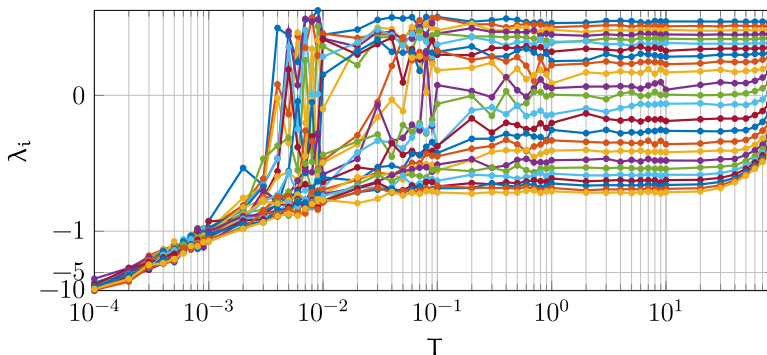16: **return** $\{\lambda_i\}$.
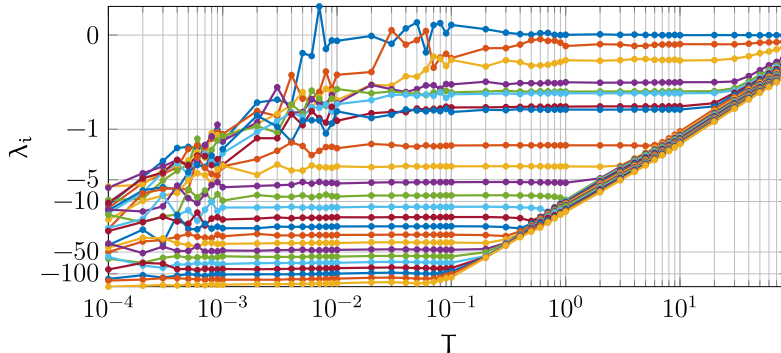
FIGURE 3. The $m = 24$ most positive Lyapunov exponents λ_i for (top) $L = 20$ and (bottom) $L = 100$ calculated using Algorithm 1 with odd-periodic boundary conditions (2.3) and different interval times T. An accurate Lyapunov exponent is approximately constant as T varies. When $L = 20$ there is no range of T for which *all* 24 exponents are constant, but the most negative ones are least important. For $L = 100$, all $m = 24$ Lyapunov exponents are reasonably constant for $1 < T < 10$.

In implementing Algorithm 1 for the Kuramoto–Sivashinsky PDE (2.1) an n-dimensional approximate system is used, either spectral in space for the periodic case (2.2) or finite differences for the odd-periodic case (2.3). In either case we choose truncations so that the maximum wavenumber resolved was $k_{\max} \approx 9$ (which decays extremely rapidly, on a time scale of $1/k_{\max}^4 \approx 10^{-4}$). Initial conditions were random and normally distributed $\sim \mathcal{N}(0, 1)$. After some testing of different transient times τ, we selected $\tau = 2000$, which is smaller than some other studies (for example, Wittenberg and Holmes [35] used $\tau = 100\,000$), but repeatedly provided consistent and expected dynamics. A total of $N = 1000$ reorthonormalization steps are performed in the exponent computations. This choice of N computes fairly accurate Lyapunov exponents within a reasonable time frame.

An important decision in the numerical calculation of the Lyapunov spectrum is the size of each time interval T between reorthonormalizations. Figure 3 demonstrates

how the choice of interval T in Algorithm 1 affects the calculation of the $m = 24$ most positive Lyapunov exponents, for small domain $L = 20$ or large domain $L = 100$, in the case of odd-periodic boundary conditions (2.3) (the periodic case (2.2) provides similar plots). For a small interval T ($T \lesssim 0.1$ for $L = 20$, and $T \lesssim 1$ for $L = 100$) the most positive Lyapunov exponents are inaccurate, because T is too small to sufficiently capture the trajectory divergence, leading to an unstable QR decomposition. For larger interval T ($T \gtrsim 0.1$ for $L = 20$, and $T \gtrsim 10$ for $L = 100$), the most negative of the $m = 24$ Lyapunov exponents evolve for too long and are corrupted towards the more positive exponents. Based upon Figure 3 we generally chose reorthonormalization interval $T = 2$. With this choice of T we accurately resolve the most positive Lyapunov exponents, while also computing a sufficient number of negative Lyapunov exponents for the evaluation of the Kaplan–Yorke dimension for the chosen range of domains.

Figures 4 and 5 plot the 24 most positive Lyapunov exponents for the Kuramoto–Sivashinsky PDE (2.1) over different domain sizes, $0 < L \leq 100$, with periodic (2.2) and odd-periodic (2.3) boundary conditions, respectively. Although these calculations of the Lyapunov exponents contain noise, the exponents generally increase as L increases, and larger values of L generally have more positive exponents. However, the increase in the Lyapunov exponents is limited as they appear to be bounded above by about 0.1, for both the periodic and odd-periodic cases. This upper bound 0.1 matches with the upper bound observed for the rigid boundary condition case [23, 37].

We now further explore the Lyapunov exponents in the periodic case. The structure of the positive Lyapunov exponents is noisy, but there are some reasonably clear trends: here we show that the ith positive Lyapunov exponent on a domain length L is approximately

$$\lambda_i(L) \approx 0.093 - 0.94(i - 0.39)/L. \tag{3.2}$$

To derive this approximation, first look at the i-dependence for various fixed L: Figure 6 plots the median of Lyapunov exponent $\lambda_i(L)$ for fixed L as a function of index i. The median of Lyapunov exponent $\lambda_i(L)$ accounts for the noisy data in Figure 4 and is defined as the median of $\lambda_i(x)$ over the interval $x \in [L - 1, L + 1]$ (21 data points). Then the vertical bars for each point represent plus and minus the mean absolute deviation (MAD) over the domain of x: these statistics are more robust to outliers than the usual mean and standard deviation, and so appear to be more suitable here. Figure 6 indicates that the Lyapunov exponents are, for fixed L, approximately equispaced in i, especially for $i \leq 5$.

In Figure 6 the magnitude of the slope of the i-dependence decreases as the domain length L increases, so we try to fit a function of the power-law form $\lambda_i(L) \approx a + (b + ci)/L^p$ for various exponents p. Figure 7 plots the residual error in the fit as a function of exponent p, showing that there is a minimum error at $p \approx 1$; this minimum occurs both in the rout mean square error and the MAD error. In view of the fluctuations in the MAD, it seems reasonable to choose the case of the exponent $p = 1$ reported by equation (3.2). Moreover, this is the exponent which best fits our preconception that the chaos in the Kuramoto–Sivashinsky PDE is "extensive": that the number of positive Lyapunov exponents increases linearly with domain length L.
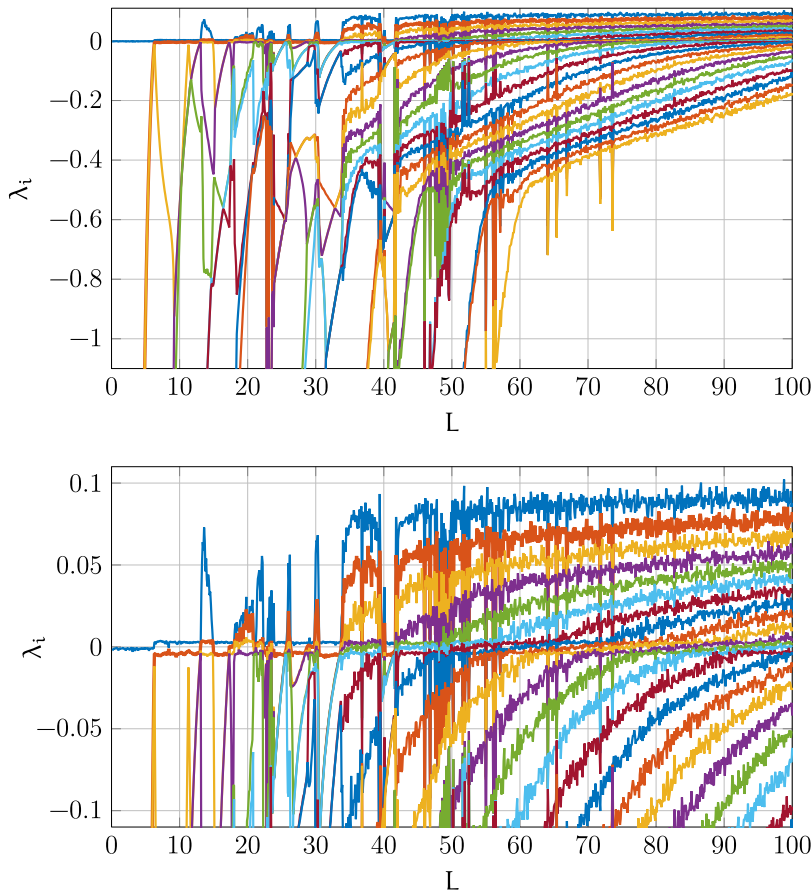
FIGURE 4. The 24 most positive Lyapunov exponents $\lambda_1, \lambda_2, \ldots, \lambda_{24}$, computed for the Kuramoto–Sivashinsky PDE (2.1) on the periodic (2.2) spatial domain for domain sizes $0 < L \leq 100$. The bottom plot provides a more detailed look at those Lyapunov exponents near zero.

Section 4 explores this issue further via the Kaplan–Yorke dimension, and finds results consistent with the approximate formula (3.2).

4. Compute the Kaplan–Yorke dimension

The Kaplan–Yorke dimension is a measure of the dimension of an attractor [18], and is defined in terms of a sum of the most positive Lyapunov exponents

$$D_{\mathrm{KY}} = j + \frac{\sum_{i=1}^{j} \lambda_i}{|\lambda_{j+1}|}, \tag{4.1}$$

where j is the largest index such that $\sum_{i=1}^{j} \lambda_i \geq 0$. The Kaplan–Yorke dimension is an upper bound of the Hausdorff dimension of the attractor, and as each of the
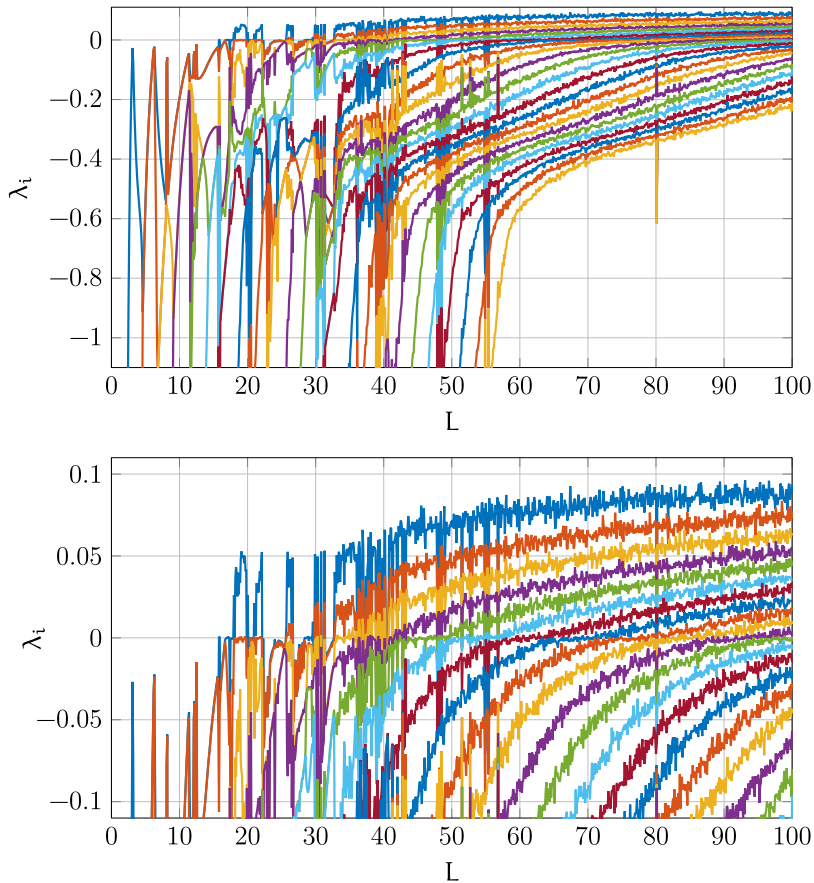
FIGURE 5. The 24 most positive Lyapunov exponents $\lambda_1, \lambda_2, \ldots, \lambda_{24}$, computed for the Kuramoto–Sivashinsky PDE (2.1) on the odd-periodic (2.3) spatial domain for domain sizes $0 < L \leq 100$. The bottom plot provides a more detailed look at those Lyapunov exponents near zero.

j Lyapunov exponents corresponds to an orthogonal direction, the Kaplan–Yorke dimension approximates the minimum number of modes required to describe the emergent dynamics of the system on the attractor [12].

In formula (4.1), the term $\sum_{i=1}^{j} \lambda_i / |\lambda_{j+1}|$ is usually a fraction in $(0, 1)$ and so the index j is roughly the Kaplan–Yorke dimension. Using the approximation (3.2) to the Lyapunov exponents for the periodic case, one may straightforwardly estimate the j for which $\sum_{i=1}^{j} \lambda_i \approx 0$, namely, $j \approx 0.2L - 0.2$. This is acceptably close to the Kaplan–Yorke dimension, $D_{KY} \approx 0.226\,L - 0.160$, shown in Figure 8 and obtained from extensive computation. The Kaplan–Yorke dimension does not always follow this linear trend, particularly at low domain sizes $L \lesssim 50$, indicating stable or less chaotic regions among the general trend of increasing chaos with domain size L. For larger domain sizes $L \gtrsim 50$ we observe only a few sharp localized deviations from the
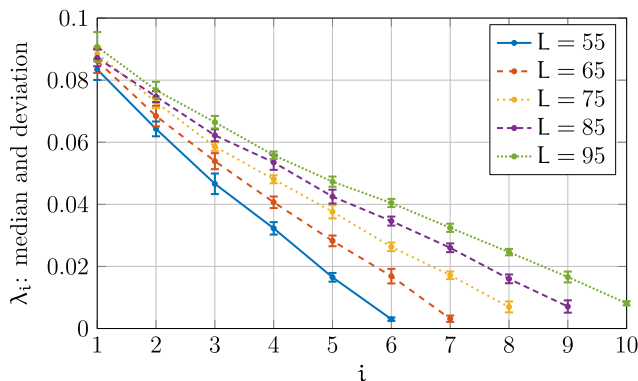
FIGURE 6. Positive Lyapunov exponents λ_i for the periodic case (2.2), Figure 4, as a function of index i. The joining lines are purely to aid visualization. For each L the data point plotted is the median of $\lambda_i(x)$ over the window $x \in [L-1, L+1]$, with error bars indicating plus and minus the mean absolute deviation over the domain of x.
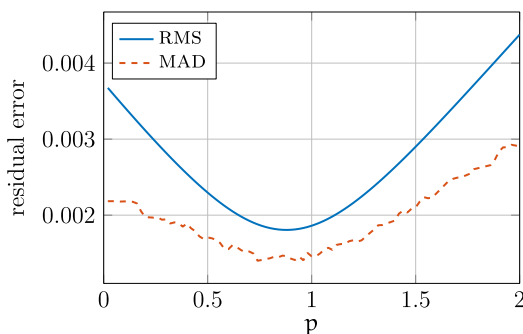

FIGURE 7. Fit the Lyapunov exponents $\lambda_i(L) \approx a + (b + ci)/L^p$ for various exponents p and then plot the residual error as a function of exponent p: here the root mean square error (RMS) and the mean absolute deviation (MAD). The minima of these curves suggest the optimum exponent $p \approx 1$.

linear trend (for example, $L \approx 64.1$ and $L \approx 80.1$ for the periodic and non-periodic cases, respectively). We interpret these localized deviations at larger L as indicative of small windows of less chaotic dynamics [5].

Table 1 presents Lyapunov exponents and Kaplan–Yorke dimensions for six different periodic domain sizes $L = 12, 13.5, 22, 36, 60, 100$ (the case $L = 22$ is chosen for comparison with the Lyapunov exponents of Cvitanović et al. [5]: our Lyapunov exponents agree with theirs to a difference of about 0.002), whereas Table 2 presents Lyapunov exponents and Kaplan–Yorke dimensions for six different odd-periodic domain sizes $L = 17.5, 18.1, 18.2, 41, 60, 100$. These tables demonstrate how the increasingly positive Lyapunov exponents reveal the onset of chaotic dynamics and the increasing dimension of the chaotic attractor. These calculations of the Lyapunov exponents and Kaplan–Yorke dimensions with odd periodic domains are compatible with previously calculated Kaplan–Yorke dimensions [25].

- periodic boundary conditions (2.2)
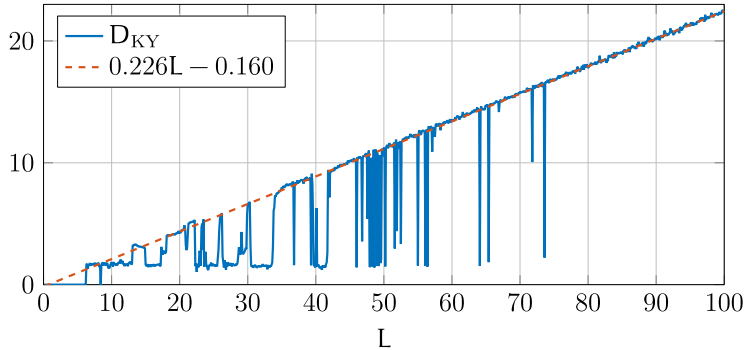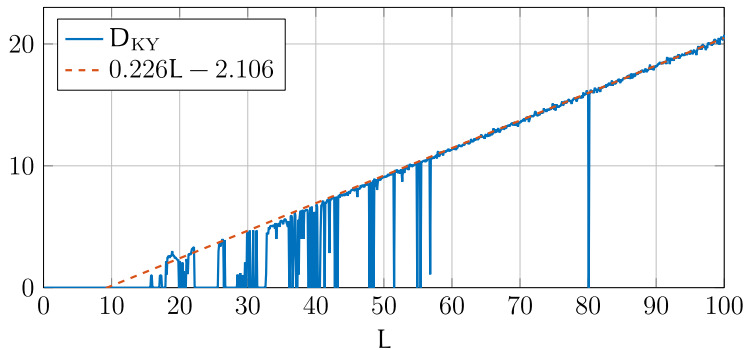

- odd-periodic boundary conditions (2.3)

FIGURE 8. The Kaplan–Yorke dimension D_{KY} dependence on domain size L, computed for the Kuramoto–Sivashinsky PDE (2.1) on (top) the periodic spatial domain (2.2), and (bottom) the odd-periodic spatial domain (2.3). In both cases, the Kaplan–Yorke dimension increases linearly with the domain size L, with $D_{KY} \approx 0.226L - c$ for $c = 0.160$ and 2.106, respectively. This linearity appears most accurate for larger domains, $L \gtrsim 80$. At lower domain sizes, (top) $L \lesssim 80$ and (bottom) $L \lesssim 60$, there are several non-chaotic regions where the Kaplan–Yorke dimension is not of interest.

Figure 8 shows that as the domain size L increases, the Kaplan–Yorke dimension scales linearly with $D_{KY} \propto 0.226L$ for sufficiently large L ($L \gtrsim 80$). Similarly, in the case of rigid boundary conditions $u, \partial_x u = 0$ at $x = 0$ and at $x = L$, both Manneville [23] and Tajima and Greenside [33] found the Kaplan–Yorke dimension to scale as $0.230L$ when $50 < L < 400$. The small 2% difference in the coefficient suggests that the scaling of the Kaplan–Yorke dimension for the Kuramoto–Sivashinsky PDE (2.1) on domain sizes $L \gtrsim 80$ only depends on the nature of the given boundary condition through an additive constant. In contrast, for smaller domain sizes $L \lesssim 50$, all points in the domain are somewhat close to a boundary, and boundary effects play a more dominant role in the dynamics. The linear scaling of the attractor, here measured with the Kaplan–Yorke dimension, is a defining feature of an extensively chaotic system [4, 13].

TABLE 1. The 12 most positive Lyapunov exponents and the Kaplan–Yorke dimension for several domain sizes L and periodic boundary conditions (2.2).

	$L = 12$	$L = 13.5$	$L = 22$	$L = 36$	$L = 60$	$L = 100$
λ_1	0.003	0.059	0.043	0.080	0.089	0.088
λ_2	−0.005	0.004	0.003	0.056	0.067	0.082
λ_3	−0.088	−0.004	0.002	0.014	0.055	0.070
λ_4	−0.089	−0.227	−0.004	0.003	0.041	0.061
λ_5	−0.186	−0.730	−0.008	−0.003	0.030	0.048
λ_6	−3.524	−1.467	−0.185	−0.004	0.005	0.041
λ_7	−3.525	−1.529	−0.253	−0.021	0.003	0.033
λ_8	−9.835	−6.956	−0.296	−0.088	0.000	0.028
λ_9	−9.849	−6.963	−0.309	−0.160	−0.004	0.018
λ_{10}	−9.959	−7.977	−1.965	−0.224	−0.009	0.012
λ_{11}	−10.01	−7.993	−1.967	−0.309	−0.029	0.005
λ_{12}	−10.12	−9.199	−5.599	−0.373	−0.066	0.003
D_{KY}	1.663	3.259	5.198	8.229	13.56	22.44

TABLE 2. The 12 most positive Lyapunov exponents and the Kaplan–Yorke dimension for several domain sizes L and odd-periodic boundary conditions (2.3).

	$L = 17.5$	$L = 18.1$	$L = 18.2$	$L = 41$	$L = 60$	$L = 100$
λ_1	−0.001	0.000	0.036	0.067	0.076	0.094
λ_2	−0.166	−0.003	−0.001	0.038	0.056	0.077
λ_3	−0.272	−0.194	−0.073	0.017	0.042	0.063
λ_4	−0.299	−0.280	−0.268	0.001	0.027	0.056
λ_5	−0.300	−0.377	−0.359	−0.008	0.021	0.044
λ_6	−0.526	−4.813	−4.044	−0.029	0.006	0.036
λ_7	−0.619	−4.923	−4.348	−0.076	0.000	0.031
λ_8	−1.794	−1.391	−1.395	−0.162	−0.007	0.022
λ_9	−3.780	−3.145	−3.070	−0.237	−0.029	0.017
λ_{10}	−6.513	−5.525	−5.383	−0.283	−0.050	0.008
λ_{11}	−9.692	−8.700	−8.538	−0.318	−0.094	0.001
λ_{12}	−9.854	−9.540	−10.10	−0.355	−0.146	0.000
D_{KY}	0.000	1.081	2.482	7.056	11.35	20.75

5. Conclusion

Through an exhaustive computation and analysis of the positive and least negative Lyapunov exponents, we investigated the development of spatio-temporal chaos in the Kuramoto–Sivashinsky PDE (2.1) as the domain size L increases. We found new details of how the Lyapunov exponents and the Kaplan–Yorke dimension increase with

domain size, and are able to identify successive transitions into more chaotic regimes as individual Lyapunov exponents change sign from negative to positive, indicating additional directions in which trajectories of the chaotic system diverge.

The spatial extensivity of the Kuramoto–Sivashinsky PDE (2.1) that we have confirmed here in new detail indicates that the system in a large domain may be viewed as composed of interacting subsystems, approximately uncorrelated for short enough times [13, 35, 37]. This interpretation suggests that we should be able to successfully simulate the "turbulence" in the Kuramoto–Sivashinsky PDE (2.1) on very large domains by appropriately coupling relatively small patches of simulations across space using the equation-free paradigm [20]. Exactly what may be an appropriate coupling is the subject of ongoing research.

Acknowledgements

References

[1]   G. Benettin, L. Galgani, A. Giorgilli and J.-M. Strelcyn, "Lyapunov characteristic exponents for smooth dynamical systems and for hamiltonian systems; a method for computing all of them. Part 2. Numerical application", *Meccanica* **15** (1980) 21–30; doi:10.1007/BF02128237.

[2]   R. Chertovskih, E. V. Chimanski and E. L. Rempel, "Route to hyperchaos in Rayleigh–Bénard convection", *Europhys. Lett.* **112** (14001); doi:10.1209/0295-5075/112/14001.

[3]   C. Chicone, *Ordinary differential equations with applications*, Volume 34 *Texts in Applied Mathematics* (Springer, New York, 2006); doi:10.1007/0-387-35794-7.

[4]   M. C. Cross and P. C. Hohenberg, "Hohenberg. Pattern formation outside of equilibrium", *Rev. Mod. Phys.* **65** (1993) 851–1112; doi:10.1103/RevModPhys.65.851.

[5]   P. Cvitanović, R. Davidchack and E. Siminos, "On the state space geometry of the Kuramoto–Sivashinsky flow in a periodic domain", *SIAM J. Appl. Dyn. Syst.* **9** (2010) 1–33; doi:10.1137/070705623.

[6]   H. Dankowicz, P. Holmes, G. Berkooz and J. Elezgaray, "Local models of spatio-temporally complex fields", *Physica* D **90** (1996) 387–407; doi:10.1016/0167-2789(95)00245-6.

[7]   L. Dieci, R. Russell and E. Van Vleck, "On the computation of Lyapunov exponents for continuous dynamical systems", *SIAM J. Numer. Anal.* **34** (1997) 402–423; doi:10.1137/S0036142993247311.

[8]   J.-P. Eckmann and D. Ruelle, "J. Ergodic theory of chaos and strange attractors", *Rev. Mod. Phys.* **57** (1985) 617–656; doi:10.1103/RevModPhys.57.617.

[9]   V. M. Eguíluz, P. Alstrøm, E. Hernández-García and O. Piro, "Average patterns of spatiotemporal chaos: a boundary effect", *Phys. Rev.* E **59** (1999) 2822–2825; doi:10.1103/PhysRevE.59.2822.

[10] C. Foias, B. Nicolaenko, G. R. Sell and R. Temam, Inertial manifolds for the Kuramoto–Sivashinsky equation and an estimate of their lowest dimension", Technical Report, University of Minnesota Digital Conservancy, 1986, http://hdl.handle.net/11299/4494.

[11] K. Geist, U. Parlitz and W. Lauterborn, "Comparison of different methods for computing Lyapunov exponents", *Prog. Theor. Phys.* **83** (1990) 875–893; doi:10.1143/PTP.83.875.

[12] P. Grassberger and I. Procaccia, "Measuring the strangeness of strange attractors", *Physica* D **9** (1983) 189–208; doi:10.1016/0167-2789(83)90298-1.

[13] H. S. Greenside, "Spatiotemporal chaos in large systems: the scaling of complexity with size", Technical Report, 1996; https://arxiv.org/abs/chao-dyn/9612004.

[14] M. Hassanaly and V. Raman, "Ensemble-LES analysis of perturbation response of turbulent partially-premixed flames", *P. Combust Inst.* **37** (2018) 2249–2257; doi:10.1016/j.proci.2018.06.209.

[15] P. C. Hohenberg and B. I. Shraiman, "Chaotic behavior of an extended system", *Physica* D **37** (1989) 109–115; doi:10.1016/0167-2789(89)90121-8.

[16] J. M. Hyman and B. Nicolaenko, "The Kuramoto–Sivashinsky equation: a bridge between PDEs and dynamical systems", *Physica* D **18** (1986) 113–126; doi:10.1016/0167-2789(86)90166-1.

[17] J. M. Hyman, B. Nicolaenko and S. Zaleski, "Order and complexity in the Kuramoto–Sivashinsky model of weakly turbulent interfaces", *Physica* D **23** (1986) 265–292; doi:10.1016/0167-2789(86)90136-3.

[18] J. L. Kaplan and J. A. Yorke, "Chaotic behavior of multidimensional difference equations", in: *Functional differential equations and approximation of fixed points* (eds H.-O. Peitgen and H.-O. Walther), (Springer, Berlin, 1979) 204–227; doi:10.1007/BFb0064319.

[19] L. Keefe, P. Moin and J. Kim, "The dimension of attractors underlying periodic turbulent Poiseuille flow", *J. Fluid Mech.* **242** (1992) 1–29; doi:10.1017/S0022112092002258.

[20] I. G. Kevrekidis and G. Samaey, "Equation-free multiscale computation: algorithms and applications", *Annu. Rev. Phys. Chem.* **60** (2009) 321–344; doi:10.1146/annurev.physchem.59.032607.093610.

[21] Y. Kuramoto and T. Tsuzuki, "Persistent propagation of concentration waves in dissipative media far from thermal equilibrium", *Prog. Theor. Phys.* **55** (1976) 356–369; doi:10.1143/PTP.55.356.

[22] Y. Lan and P. Cvitanović, "Unstable recurrent patterns in Kuramoto–Sivashinsky dynamics", *Phys. Rev. E* **78** (2008) 026208; doi:10.1103/PhysRevE.78.026208.

[23] P. Manneville, "Liapounov exponents for the Kuramoto–Sivashinsky model", in: *Macroscopic modelling of turbulent flows* (eds U. Frisch, J. B. Keller, G. C. Papanicolaou and O. Pironneau), (Springer, Berlin, 1985) 319–326; doi:10.1007/3-540-15644-5 26.

[24] Y. Pomeau and S. Zaleski, "The Kuramoto–Sivashinsky equation: a caricature of hydrodynamic turbulence?" in: *Macroscopic modelling of turbulent flows* (eds U. Frisch, J. B. Keller, G. C. Papanicolaou and O. Pironneau), (Springer, Berlin, 1985) 296–303; doi:10.1007/3-540-15644-5 23.

[25] E. L. Rempel, A. C.-L. Chian, E. E. N. Macau and R. R. Rosa, "Analysis of chaotic saddles in high-dimensional dynamical systems: the Kuramoto–Sivashinsky equation", *Chaos* **14** (2004) 545–556; doi:10.1063/1.1759297.

[26] D. Ruelle, "Ergodic theory of differentiable dynamical systems", *Publ. Math. Inst. Hautes Études Sci.* **50** (1979) 27–58; doi:10.1007/bf02684768.

[27] D. Ruelle and F. Takens, "On the nature of turbulence", *Commun. Math. Phys.* **20** (1971) 167–192; doi:10.1007/BF01646553.

[28] I. Shimada and T. Nagashima, "A numerical approach to ergodic problem of dissipative dynamical systems", *Prog. Theor. Phys.* **61** (1979) 1605–1616; doi:10.1143/PTP.61.1605.

[29] G. I. Sivashinsky, "Nonlinear analysis of hydrodynamic instability in laminar flames–I. Derivation of basic equations", *Acta Astron.* **4** (1977) 1177–1206; doi:10.1016/0094-5765(77)90096-0.

[30] G. I. Sivashinsky and D. M. Michelson, "On irregular wavy flow of a liquid film down a vertical plane", *Prog. Theor. Phys.* **63** (1980) 2112–2114; doi:10.1143/PTP.63.2112.

[31] C. Skokos, "The Lyapunov characteristic exponents and their computation", in: *Dynamics of small solar system bodies and exoplanets* (eds J. J. Souchay and R. Dvorak), (Springer, Berlin, 2010) 63–135; doi:10.1007/978-3-642-04458-8_2.

[32] J. C. Sprott, *Elegant chaos: algebraically simple chaotic flows* (World Scientific, Singapore, 2010); doi:10.1142/7183.

[33] S. Tajima and H. S. Greenside, "Microextensive chaos of a spatially extended system", *Phys. Rev. E* **66** (2002) 017205; doi:10.1103/PhysRevE.66.017205.

[34] F. Takens, *Detecting strange attractors in turbulence*, *Lect. Notes in Math.* (Springer, Berlin, 1981) 366–381; doi:10.1007/bfb0091924.

[35]   R. W. Wittenberg and P. Holmes, "Scale and space localization in the Kuramoto–Sivashinsky equation", *Chaos* **9** (1999) 452–465; doi:10.1063/1.166419.

[36]   M. Xu, "Spatiotemporal chaos in large systems driven far-from-equilibrium: connecting theory with experiment", Ph. D. Thesis, Virginia Polytechnic Institute and State University, 2017. https://vtechworks.lib.vt.edu/handle/10919/79499.

[37]   H.-L. Yang, K. A. Takeuchi, F. Ginelli, H. Chaté and G. Radons, "Hyperbolicity and the effective dimension of spatially extended dissipative systems", *Phys. Rev. Lett.* **102** (2009) 074102; doi:10.1103/PhysRevLett.102.074102.21.